Particle Characterization Using Multiple Scattering Decorrelation Methods. Part 1: Standard Latex Particles

Christian Sinn, Ralf Niehüser, Ekkehard Overbeck, Thomas Palberg*

(Received: 15 October 1998; resubmitted: 23 March 1999)

Abstract

We determined the dimensions of standard polystyrene latex spheres suspended in water at different sample concentrations by dynamic light scattering and turbidimetry. Applying two different schemes for the decorrelation of multiple scattering, we show that the samples exhibit distortions of the auto-correlation function due to multiple scattering even at moderate volume fractions, which prohibits the correct determination of the particle radius. The cross-correlation functions, however, are free from these distortions. The recently deployed three-dimensional cross-correlation setup is superior to the commercially available two-color machine, as more turbid samples are accessible. In order to verify the results obtained by dynamic light scattering, we performed turbidity measurements with the same samples. This method is inherently free from multiple scattering contributions. We observe a systematically smaller radius in turbidimetry than in dynamic light scattering. The deviation, however, is only slightly outside the accuracy range of the measurements. We discuss possible origins for this deviation and show that our measurements are compatible with a hairy layer present on the particle's surface.

1 Introduction

In fundamental research, there is a great demand for the experimental investigation of highly concentrated colloidal suspensions that serve as model systems for structural and dynamic aspects of the behavior of condensed matter [1]. Theoretical progress permits even the comprehension of hydrodynamic interactions [2], which, being a many-body effect, are difficult to describe. Characteristic differences between a hard-sphere pair potential and the Yukawa pair potential, valid for charge-stabilized suspensions, have become visible [3]. From an experimental point of view, polystyrene latex spheres in aqueous suspensions are well suited for such investigations, as their interaction potential can be tuned very efficiently by adjusting the ionic strength of the suspensions, controlled by conductivity measurements. The main disadvantage of these systems is their strong (multiple) scattering even at moderate concentrations, *i.e.* volume fractions $\phi > 10^{-3}$.

Significant progress has been achieved in the experimental suppression of multiple scattering contributions from dynamic light scattering (DLS) data [4]. It is this achievement that makes the determination of characteristic particle dimensions viable, even in cases where multiple scattered light dominates the measured intensity. This decorrelation of multiple scattering is applicable not only to colloidal suspensions of high concentration, but also to turbid media in general, for example liquid mixtures approaching a critical point.

Recently, a survey of different methods to determine the particle size in dilute suspensions has been published [5]. In addition, a sophisticated single particle tracking experiment has been applied to yield particle size distributions [6]. In this work, we exploited light scattering methods free from multiple scattering contributions for the careful determination of the radius of spherical standard latex particles suspended in water. The paper is organized as follows. After a short description of the sample preparation, we outline the technique of multiple scattering decorrelation and give an overview of the radii we determined from samples of differing concentration. This is followed by a description of careful turbidity measurements and their results. We finish with a thorough discussion of side-effects that influence the determination of particle radii by the methods applied in this investigation.

2 Sample Preparation

We used polystyrene latex particles with a nominal particle diameter of 0.12 µm as supplied by IDC Corp., USA (Batch No. 10-202-66). The particle diameter has been determined by transmission electron microscopy; its coefficient of variation is stated to be 4.7%.

For the sample preparation, the slightly diluted raw suspension was brought into contact with a mixed-bed ion-exchange resin (Amberlite UP-604, Rohm & Haas, USA), in order to remove ionic impurities from the solutions. This contact is usually accompanied by a (reversible) aggregation process of the particles at the surface of the ion-exchange resin. After a few days, we passed the suspension through 5 µm filters in order to remove aggregates and resin debris. We determined the volume fraction of this filtered stock suspension after drying a small portion at elevated temperature (50°C) by careful weighing of the polymer film

* Dr. *C. Sinn*, *R. Niehüser*, *E. Overbeck*, Prof. Dr. *T. Palberg*, Institut für Physik der Johannes-Gutenberg-Universität, Staudingerweg 7, D-55099 Mainz (Germany).

© WILEY-VCH Verlag GmbH, D-69451 Weinheim, 1999

0721-3115/99/95–101 $17.50+.50/0

obtained. The density of the latex particles ($\rho = 1.055\,\mathrm{g\,cm^{-3}}$) was used as given by the supplier.

We prepared the samples by diluting the stock suspension with deionized water from a Milli-Q water source (Millipore, USA) with added NaCl to obtain a foreign salt concentration of $c_s = 0.5\,\mathrm{mmol\,dm^{-3}}$ in every sample. Care was taken to prevent the particles from coming into contact with salt concentrations higher than $1\,\mathrm{mmol\,dm^{-3}}$ in this procedure in order to avoid irreversible particle aggregation.

3 Decorrelation of Multiple Scattering

The main aim of this contribution is to demonstrate experimentally the benefits of the recently developed DLS cross-correlation techniques for applications in particle sizing in highly concentrated suspensions. The theoretical principles of multiple scattering decorrelation have been described in detail by *Schätzel* [4]. Details of different experimental setups have been described elsewhere [7, 8]. We therefore restrict ourselves here to explaining only schematically the "evolution" of DLS.

Figure 1a shows the wavevector arrangement of a usual DLS setup. The incoming and scattered wavevectors, $\vec{k}_i$ and $\vec{k}_f$, respectively, include the scattering angle θ, where the scattering vector $\vec{q} = \vec{k}_i - \vec{k}_f$ defines the spatial scale of the scattering experiment.

Multiple scattering contributions to temporal correlation functions can be decorrelated by performing simultaneously two geometrically different scattering experiments that share a common scattering volume at identical $\vec{q}$. If the temporal intensity fluctuations are cross-correlated, multiply scattered light is (in general) determined at a different $\vec{q}$ than singly scattered light and therefore uncorrelated.

In case of the two-color scheme (Figure 1b), the two independent experiments are realized by two light beams of different wavelength that include a small difference angle δ_{2C}. Appropriate narrow bandwidth filters in front of the detectors separate the wavelengths. Usually, a multi-line Ar^+ laser is deployed, using the main $\lambda_1 = 514.5\,\mathrm{nm}$ and $\lambda_2 = 488.0\,\mathrm{nm}$ wavelengths; the cross-correlation function then is obtained at the (virtual) mean wavelength $\lambda = 501.3\,\mathrm{nm}$. This setup benefited from ideas proposed by *Phillies* [9] and *Dhont* and *de Kruif* [10] and was realized in the laboratory of *Schätzel* in Kiel [11]. The machine is now available commercially; its merits for the characterization of colloidal samples have been described impressively [7].

Following a suggestion by *Schätzel* (*cf.* Ref. [4]), we realized in our laboratory an alternative machine called a 3D setup [8], the wavevector scheme of which is shown in Figure 1c. The two independent experiments are separated spatially, thereby eliminating any restrictions on the wavelengths used. Consequently, we take advantage of long-wavelength semiconductor diode lasers working at $\lambda = 788.7\,\mathrm{nm}$, as the scattering cross-section is drastically reduced compared with the blue-green laser for the two-color scheme. Comparable equipment is available in different laboratories [12, 13].

Two main differences between the two-color setup and the 3D setup are worth mentioning. First, there is no need for a readjustment of the difference angle δ_{3D} with scattering angle θ, in contrast to δ_{2D}. This makes the 3D setup less complicated and easier to align. Second, though, because the different experiments cannot be separated by any kind of filter, uncorrelated light contributes to the cross-correlation function and reduces the signal-to-noise ratio of the 3D setup. A detailed discussion of this effect can be found in Ref. [8]. Whereas for the two-color experiment only standard cylindrical cuvettes with an inner diameter of not less than 10 mm can be used for optical reasons, for the 3D setup rectangular cuvettes can be employed. The amount of multiply scattered light decreases with decreasing thickness of the cuvette. A cuvette thickness of 1 mm has been applied successfully [8, 14].

Figure 2 to Figure 5 show the DLS results for the particles under study. For simplicity, we restrict ourselves here to a description of the results obtained at a single scattering angle, which is slightly different for the two methods. The correlation functions were recorded using an ALV-5000/E correlator. Ten correlation functions lasting 30 s each were averaged.

Figure 2 shows intensity auto- and cross-correlation functions obtained from a sample with $\phi = 10^{-3}$ using the two-color setup. The two auto-correlation functions for both wavelengths clearly show an upswing at small lag times, which is a mere artifact due to multiple scattering contributions. The decrease in the scattering cross-section with wavelength manifests itself impressively in smaller distortions for the green wavelength as compared with the blue wavelength. The cross-correlation function, in turn, is free

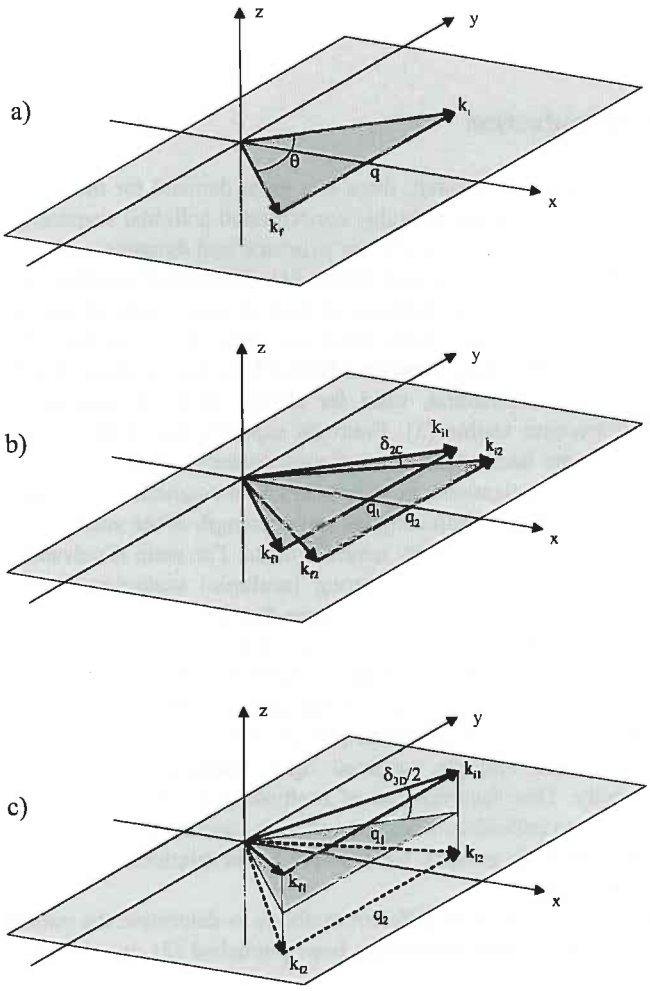

Fig. 1: "Evolution" of dynamic light scattering. (a) Conventional setup, with initial and final wavevectors $\vec{k}_i$ and $\vec{k}_f$, respectively. (b) Two-color setup; initial and final wavevectors both include a difference angle δ_{2C}; $\lambda_1 = 514.5\,\mathrm{nm}$, $\lambda_2 = 488.0\,\mathrm{nm}$. (c) 3D setup; the wavevectors include a difference angle δ_{3D} and share the common wavelength $\lambda = 788.7\,\mathrm{nm}$.

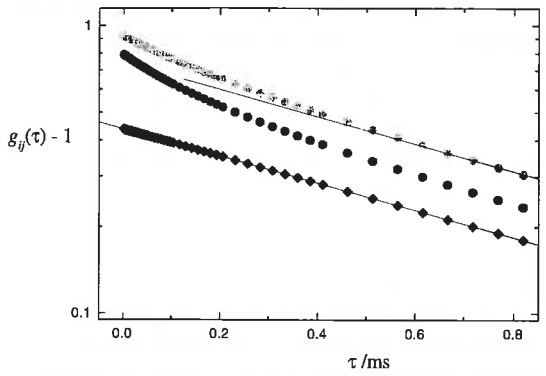

Fig. 2: Intensity auto-correlation functions ($g_{11}(\tau)$, light-gray circles, and $g_{22}(\tau)$, dark-gray circles) and cross-correlation function ($g_{12}(\tau)$, black diamonds) obtained with the two-color apparatus. The sample volume fraction was $\phi = 10^{-3}$. The scattering angle is $\theta = 45°$, the scattering vector is $q = 12.8\,\mu m^{-1}$ with $\lambda = 501.3$ nm and $n = 1.334$. The straight line through $g_{12}(\tau)$ is a fit to a single exponential which yields $R = 64.5$ nm. For comparison, this fit curve has been shifted to the data points of $g_{11}(\tau)$.

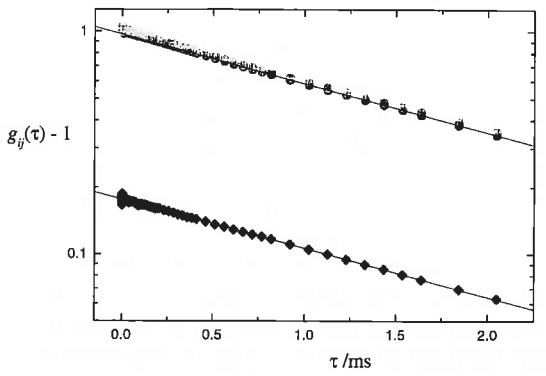

Fig. 3: Intensity auto-correlation functions ($g_{11}(\tau)$, light-gray circles, and $g_{22}(\tau)$, dark-gray circles) and cross-correlation function ($g_{12}(\tau)$, black diamonds) obtained with the 3D apparatus. The sample volume fraction was $\phi = 10^{-3}$. The scattering angle is $\theta = 48°$, the scattering vector is $q = 8.7\,\mu m^{-1}$ with $\lambda = 788.7$ nm and $n = 1.328$. The straight line through $g_{12}(\tau)$ is a fit to a single exponential which yields $R = 63.4$ nm. For comparison, this fit curve has been shifted to the data points of $g_{22}(\tau)$.

from any visible distortion. The signal-to-noise ratio decreases as explained above, because the multiple scattered light is decorrelated and contributes to the baseline only.

Qualitatively the same result can be seen in Figure 3, where the same sample was investigated using the 3D scheme. Note that the auto-correlation functions determined by both detectors are again distorted, but to a lesser extent owing to the longer wavelength used. The cross-correlation function is again free from multiple scattering distortions.

In order to evaluate the cross-correlation functions quantitatively, we fit the correlator channel contents to a second-order cumulant expansion according to

$$g_{12}(\tau) = 1 + \beta \cdot \exp(-\Gamma\tau) \qquad \text{with} \qquad \Gamma = K_1 + K_2\tau. \tag{1}$$

In the fitting process, it turned out that every cross-correlation function in this study exhibited a second cumulant of the order of the fitting errors. For simplicity, we therefore fix $K_2 = 0$, thereby assuming a simple exponential decay. We verified that K_1 is invariant upon fixing K_2. In the homodyne detection limit, we relate the first cumulant to the particle radius by standard light scattering theory [15] according to

$$K_1 = 2Dq^2 \qquad \text{and} \qquad R = \frac{k_B T}{6\pi\eta D}, \tag{2}$$

where D is the diffusion coefficient of the particles, $T = 293$K is the sample temperature and $\eta = 1.006$ mPa s is the viscosity of water at that temperature.

These fits are shown in Figure 2 and Figure 3 as straight lines, the particle radii we obtained are given in Table 1. The cross-correlation functions for every concentration we investigated are shown in Figure 4 and Figure 5. Note that the signal-to-noise ratio (the intercept β) decreases with increasing concentration, because an increasing amount of multiple scattered light is decorrelated. In addition, we note a "passing" behavior of the cross-correlation functions of the two-color scheme with respect to the 3D setup, meaning that applying the two-color scheme, the intercept decreases more strongly with increasing concentration. This is again due to the wavelength dependence of the scattering cross-section and leads to the result that the most turbid sample, *i.e.* those with a volume fraction of $\phi = 10^{-2}$, could not be investigated with the two-color scheme at all, because $\beta < 0.01$. Again, the straight lines in the plots are fits to a first-order cumulant expansion, and the calculated radii are given in Table 1.

If different correlation functions are evaluated by cumulant fits, the best comparability is obtained when the fit is limited to the same decay for every correlation function (25% of the initial value, say), irrespective of its decay rate. Technically, it is easier to limit the number of correlator channels retained for the fit, a number that accordingly varies with decay rate. We limit the fitting process to time lags above 1 μs (the fifth correlator channel) and below a certain $q^2\tau$ value. This value is determined from the correlation function of worst statistical quality and chosen to be that value where strong deviations from an exponential behavior become visible. The different number of evaluated data points with different q is visible upon comparing Figure 4 with Figure 5.

As a general result, we note that the accuracy of the diffusion coefficients (and thereby of the particle radii) obtained by DLS is limited owing to the presence of coherent or incoherent background light, produced by scratches on optical surfaces or reflections of different origin. Detector nonlinearities may also

Table 1: Particle radii of a suspension of spherical standard latex particles as obtained using different methods of determination, as indicated. The average radius was obtained directly and the first moment radius was calculated assuming a Gaussian PSD and a polydispersity of $\sigma = 4.7\%$.

	Particle radius R/nm					
Sample volume fraction ϕ	$1{\cdot}10^{-2}$	$2{\cdot}10^{-3}$	$1{\cdot}10^{-3}$	$1{\cdot}10^{-4}$	Average $\langle R\rangle$/nm	First moment $\overline{R}$/nm
2C method	–	65.1	64.5	64.7	64.8 ± 2	64.1
3D method	(60.6)	65.1	63.4	66.7	65.1 ± 2	64.4
Transmission					59 ± 2	58.7
TEM					60 ± 3	60

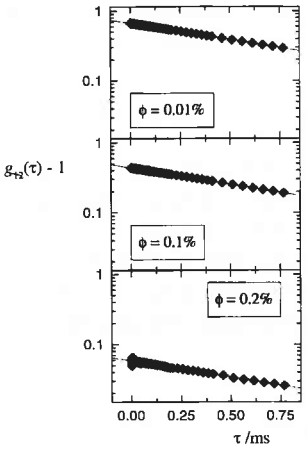

Fig. 4: Intensity cross-correlation functions obtained with the two-color apparatus for all the samples investigated. The respective volume fraction is indicated. The straight lines are fits to a single exponential; the respective radii are given in Table 1. The scattering angle was $\theta = 45°$.

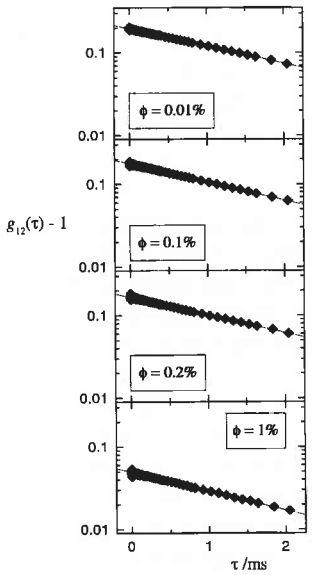

Fig. 5: Intensity cross-correlation functions obtained with the 3D apparatus for all the samples investigated. The respective volume fraction is indicated. The straight lines are fits to a single exponential; the respective radii are given in Table 1. The scattering angle was $\theta = 48°$.

have an influence on the data [16]. In addition, for strongly turbid samples, the statistical errors in determining the estimate for the true correlation function with the correlator play a role. With our temporal scheme (10 samples of a single 30 s correlator run), we obtain an accuracy of approximately $\pm 3\%$. This error is higher than the fitting error of the first cumulant, which is clearly below 1% if obtained from about 70 data points.

In Table 1 we list the calculated values for the average radius $\langle R \rangle$ obtained with each method separately. Note that every average radius is obtained from measurements at a single scattering angle, but different sample concentrations. We performed the same measurements at five different scattering angles, which are not reproduced here. The radii we obtained lay again within the 3% reproducibility range. Note, however, that we observed increasing radii with decreasing scattering angle in the 3D experiment. The effect started to be noticeable at approximately 30° and lost importance with increasing sample concentration. This effect could be clearly attributed to a small amount of coherent background light present. In accordance with this interpretation, the measured intercept decreased. It should therefore be possible to correct the radius for this effect applying the recipe of *Flammer* and *Rička* [17].

Coherent stray light definitively does not account for the small radius observed for the highest sample concentration. This value (in parentheses in Table 1) has not been included in the radius average, because we attribute its small value to structure formation within the sample. With $q = 8.6\,\mu m^{-1}$, we are well below the expected fluid structure factor maximum ($q_{max} = 14\,\mu m^{-1}$). Structure formation within the sample is expected to increase the observed diffusion coefficient for $q < q_{max}$ [18], in agreement with our measurement. Conversely, this behavior may be used to extract the static structure factor from dynamic measurements [13], a route which is of no interest for the present contribution. We conclude by saying that DLS measurements free from multiple scattering contributions yield an average radius $\langle R \rangle = (65 \pm 2)\,nm$ for the particles under study.

4 Turbidity Measurements

An alternative light scattering method to determine particle dimensions is to measure the turbidity of suspensions of the particles as a function of the concentration and to compare with scattering cross-sections calculated from exact Mie theory (Ch. 9 in Ref. [19]). This method is free from multiple scattering errors as long as the mean free photon path length is comparable to the cuvette thickness. Then, the transmitted intensity is free from contributions rescattered into the direct light path. This has to be guaranteed for medium turbid samples by placing a small pinhole in front of the detector and can be verified by comparing the measured light intensities as a function of the cuvette thickness. If Lambert-Beer's law of extinction is fulfilled (Eq. (A1.1)), the resulting turbidity is proportional to the scattering cross-section (Eq. (A1.2)). We determined the turbidity of samples with eight different particle concentrations ($\phi = 10^{-5} - 10^{-3}$) by fitting Lambert-Beer's law separately to the transmission data that were obtained employing seven different cuvette thicknesses. This extensive procedure was performed at five distinct wavelengths. The results are shown in Figure 6, where the data have been converted according to Eq. (A1.3) in order to allow for comparison with theoretical calculations.

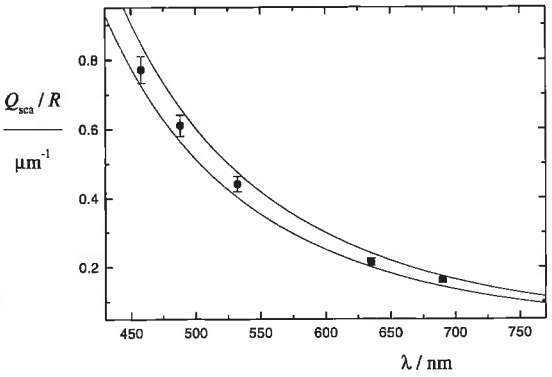

Fig. 6: Turbidity measurements converted into Q_{sca}/R according to Eq. (A1.3), as a function of the wavelength used. The data points lie within the margins of Mie calculations. Lower curve: $R = 57$ nm, upper curve: $R = 61$ nm.

The calculations were performed using the commercial program MieTab, which is based on a numerical algorithm by *Lentz* [20]; the refractive indices of water and polystyrene, and their dispersion were taken from Ref. [21]. These results are included in Figure 6 also, where two theoretical curves belonging to radii $R = 57$ and 61 nm are drawn. From Figure 6, we determine the radius of our particles to be $\langle R \rangle = (59 \pm 2)$ nm.

5 Discussion of the Results

In starting the discussion of the results, let us first say that the particle radii obtained by three different methods, *i.e.* transmission electron microscopy (TEM), turbidity measurements, and DLS applying two distinct methods for multiple scattering decorrelation, essentially agree with each other to within 5% uncertainty. However, the data clearly reveal that the DLS data yield an average particle radius that is approximately 5 nm larger than those obtained using the other two methods. If an accuracy of 3% for each method is assumed, this discrepancy is significant. In what follows we shall review known sources of deviation from the "true" particle radius for the methods utilized in this contribution.

Let us start by noting that the absolute calibration of a transmission electron microscope is uncertain to within 5% [5]. This is also the error given in Table 1 for this method. Note that the relative coefficient of variation is not prone to this uncertainty. In addition, it is known that the polystyrene particles may appear smaller in the electron microscope [22], either because the particles shrink in the vacuum chamber owing to some porosity, or the electron beam leads to some disintegration of the polymer material during the measurement.

Next, one has to be aware of the effect of polydispersity upon the measured quantity. Only a frequency count of the particles (*e.g.* applying an electron microscope or the method introduced in Ref. [6]) yields the particle size distribution (PSD) directly, the mean of which is called the number average. With any other method given, one determines a certain moment of the PSD. Therefore, only the first moments of the PSD are comparable, which can be calculated from the higher moment as obtained from the measurements using the PSD function (which, however, is usually unknown) by the calculus described in Appendix II. This calculation has been performed for the optical methods employed here. The resulting first moments are listed in the last column of Table 1. Note that the effect for the small polydispersity of the particles used in this investigation is very small. For a different situation, we refer to Ref. [22].

Let us now comment on the transmission measurements. As described in the preceding section, care has been taken that Lambert-Beer's law is fulfilled for every sample under investigation. This is crucial for transmission measurements and usually involves a check whether a smaller pinhole gives better data. In addition, highly concentrated samples give rise to structure formation even in transmission, which enables one to draw conclusions on the structure factor [23]. Although a high salt content in our samples was chosen in order to avoid structure formation, we nevertheless observed that samples with a concentration higher than $\phi > 10^{-3}$ began to deviate from Eq. (A1.3) and were therefore excluded from the analysis. As the data of our transmission measurements were obtained at five distinct wavelengths and follow closely the theoretical lines (see Figure 6), we conclude that these data are very reliable. However, the determination of the particle radius is extremely sensitive to the chosen refractive index of polystyrene, which is not known very accurately. If one allows for a 3% smaller refractive index than tabulated, the measured radius would increase to $\langle R \rangle = 64$ nm. The comparison of static light scattering data with Mie calculations therefore relies strongly on the knowledge of the refractive index of the particles under investigation, an effect which has been described already in detail [24].

DLS measurements, in contrast, are prone to different effects having an influence on the measured radii. We start with optical effects, where coherent background light increases the measured radii. For the data we have shown, however, this effect can be ruled out (see the discussion above). Multiple scattering contributions to an auto-correlation function should, in general, decrease the measured radius; this effect is absent by design for our data.

In addition, different physical effects within the sample show up in DLS. In addition to structure formation within the colloidal sample, which necessarily comes into play with increasing particle concentration but will be disregarded here, one often encounters aggregation of the particles, which can usually be detected very easily, as the measured radii decrease with increasing scattering angle. This is due to the (angle-dependent) intensity average of the DLS data. We did not observe a corresponding behavior of our data. For charge-stabilized suspensions, one also has to take into account electroviscous effects [25]. With decreasing screening of the macroion charge, any movement of the macroion involves a larger number of counterions, leading initially to a slow-down of the dynamics of the particle and hence an increase in its measured radius. This effect can be described by simply adding the Debye screening length κ^{-1} to the particle radius [26]. Even if this picture is regarded as being too simple [27, 28], the general trend can be well reproduced. In order to account for this effect, we choose $\kappa R > 4$ for our suspensions, as in this regime electroviscous effects are expected to vanish [29].

Up to this point, the colloidal particles were assumed to be rigid spheres without internal structure. Using this assumption, we described possible origins for observing a radius different from the geometrical one with the methods employed. However, recently a systematic study revealed strong evidence for the existence of a hairy layer on the surface of polystyrene latex spheres [30], an idea that had already been proposed about 20 years ago [31, 32]. We do not want to investigate here whether this concept is valid or not. We shall merely calculate whether this model can be brought into agreement with our data.

We observed that the radius measured by turbidimetry ($\overline{R} = 59$ nm) is systematically smaller than that obtained by DLS ($\overline{R} = 64$ nm). We have already mentioned that the two values coincide if the refractive index of polystyrene is assumed to be smaller by 3% than the tabulated value. As turbidity is mainly affected by the integral refractive index of the particle, one may assume that the refractive index difference originates from a 5 nm thick layer of polystyrene hairs that extend into water and ride on a compact polystyrene core with radius $R = 59$ nm. The overall extension of this core-shell object defines the hydrodynamic radius ($R = 64$ nm) measured by DLS. Assuming additivity of the refractive indices for water and polystyrene proportional to the respective volume fraction, and using the bulk refractive indices, we can calculate the water content of the shell. We obtain a water volume fraction of 83% at $\lambda = 488$ nm and 86% at $\lambda = 633$ nm. This calculation is not intended to prove the existence of a hairy layer on the surface of the particles, as the two different radii

incorporated in this calculation lie only slightly out of the uncertainty range of the measurements. We note, however, that a core-shell particle with a compact polystyrene core of radius $R = 59\,\text{nm}$ and a 5 nm thick shell of polystyrene hairs (volume fraction 15%) is compatible with our results.

In conclusion, we note that the combination of different scattering methods can provide complementary information about the sample under study, as electroviscous effects, for example, can be observed with dynamic but not with static light scattering. On the other hand, if the physics of the measurement are known in detail, suitable experiments may elucidate even slight, but systematic, incompatibilities, leading to a deeper understanding of the particle structure. However, in so doing, the statistical errors have to be carefully taken into account.

We have demonstrated the benefits of multiple scattering decorrelation for the study of concentrated suspensions. The applications that we have shown are intended to illustrate the important contribution of this technique to both fundamental and applied research in colloidal physics.

Note added in proof: Recently, a similar trend towards larger particle sizes measured with DLS was reported [33] and interpreted in terms of the shear plane connected with the electrical double layer surrounding the charge-stabilized particles. As the effect reported there seems to agree numerically with our results, the interpretation proposed in Ref. [33] may also explain our results. We note, however, that DLS measurements performed under a single scattering angle have to be interpreted with great caution.

6 Appendices

6.1 The Calculus for Turbidity Measurements

Lambert-Beer's law of extinction states the following relation between transmitted light intensity, $I(q = 0)/I_0$, turbidity τ and cuvette thickness d:

$$I(q = 0)/I_0 = \exp(-\tau d), \tag{A1.1}$$

where the turbidity is related to the particle scattering cross-section, C_{sca}, by

$$\tau = n_{\text{P}} \cdot C_{\text{sca}} = \pi R^2 \cdot n_{\text{P}} \cdot Q_{\text{sca}}, \tag{A1.2}$$

with n_{P} the particle number density in the sample and Q_{sca} the scattering cross-section normalized by the particle cross-section. As we prefer to speak about particle volume fractions $\phi = 4\pi R^3 n_{\text{P}}/3$, the measured turbidity can be compared with calculations applying

$$\tau = \frac{3}{4} \cdot \frac{Q_{\text{sca}}}{R} \cdot \phi. \tag{A1.3}$$

6.2 The Calculus for Polydispersity Effects

In order to assess the effect of polydispersity on the measured radii, we assume that the PSD can be described by a Gaussian probability distribution:

$$P(R) = \frac{1}{\sqrt{2\pi(\overline{R^2} - \overline{R}^2)}} \exp\left[-\frac{(R - \overline{R})^2}{2(\overline{R^2} - \overline{R}^2)}\right]. \tag{A2.1}$$

We note that usually slightly asymmetric PSDs are used to describe the deviations of the particle size from its mean, *e.g.* the well-known Schultz distribution. However, cases are known where the measured PSD shows a tail towards smaller radii, in contrast to the Schultz distribution [22]. As the coefficient of variation of the particle size is small in our investigation, we neglect these subtleties and note that the use of a Gaussian distribution may provide an upper limit for the polydispersity effects.

In writing the equation for $P(R)$, we used the definition for the first moment ($\overline{R}$) and second moment ($\overline{R^2}$) of a given PSD. In this contribution we identify the coefficient of variation of the particle diameter, given by the supplier, with the dimensionless standard deviation $\sigma = \left[(\overline{R^2}/\overline{R}^2) - 1\right]^{1/2}$.

It can be generally shown [34] that DLS measures the particle radius according to

$$K_1(q) \propto D = \frac{k_{\text{B}}T}{6\pi\eta\langle R\rangle} \begin{cases} \text{with } \langle R\rangle = \overline{R^6}/\overline{R^5} & \text{for } qR \to 0 \\ \text{with } \langle R\rangle = \overline{R^2}/\overline{R} & \text{for } qR \to \infty \end{cases}. \tag{A2.2}$$

We use the upper equation, as for our experiments we have $qR < 0.8$; in addition, the effect is stronger if this equation is used.

By the same calculation, transmission measurements can be shown to yield

$$I(q = 0, \langle R\rangle)/I_0 = \exp(-\tau \cdot d) \qquad \text{with} \qquad \langle R\rangle^6 = \overline{R^6}. \tag{A2.3}$$

In order to find the mean radius $\overline{R}$ (*i.e.* the first moment or central value of the Gaussian distribution) from our measurements, we calculate the relevant moment of the Gaussian distribution using Eq. (A2.2) or (A2.3), and determine that $\overline{R}$ that gives the measured radius, $\langle R\rangle$. In this procedure we fix the second moment of the distribution corresponding to the polydispersity of the particles. Note that the same procedure is possible for any functional form of the PSD, but may become numerically subtle.

7 Symbols and Abbreviations

DLS	dynamic light scattering
PSD	particle size distribution
c_{s}	foreign salt concentrations; $[c_{\text{s}}] = 1\,\text{mol}\,\text{dm}^{-3}$
C_{sca}	scattering cross section; $[C_{\text{sca}}] = 1\,\text{m}^2$
d	cuvette thickness; $[d] = 1\,\text{m}$
D	diffusion coefficient; $[D] = 1\,\text{m}^2\,\text{s}^{-1}$
$g_{ij}(\tau) = \langle I_i(t)I_j(t+\tau)\rangle/\langle I_i\rangle\langle I_j\rangle$	(normalized) intensity correlation function; $i = j$, auto-correlation; $i \neq j$, cross-correlation
I	light intensity, usually specified and of arbitrary units
k	wavevector, $k = 2\pi n/\lambda$; $[k] = 1\,\text{m}^{-1}$
k_{B}	Boltzmann's constant; $k_{\text{B}} = 1.38 \cdot 10^{-23}\,\text{J}\,\text{K}^{-1}$
K_1, K_2	first and second factor of a cumulant expansion; *cf.* Eq. (1)
n	refractive index of the suspending medium; the corresponding wavelength is specified
n_{P}	number density of colloidal particles, $n_{\text{P}} = \frac{3\phi}{4\pi R^3}$; $[n_{\text{P}}] = 1\,\text{m}^{-3}$
$P(R)$	(normalized) particle size frequency distribution (PSD); $[P(R)] = 1\,\text{m}^{-1}$
q	modulus of the scattering vector, $q = \frac{4\pi n}{\lambda} \cdot \sin\frac{\theta}{2}$; $[q] = 1\,\text{m}^{-1}$
Q_{sca}	normalized scattering cross-section, $Q_{\text{sca}} = C_{\text{sca}}/\pi R^2$

R particle radius in general; $[R] = 1\,\mathrm{m}$
$\langle R \rangle$ measured (average) particle radius
$\overline{R^n} = \int_{-\infty}^{\infty} R^n P(R)\mathrm{d}R$; $[\overline{R^n}] = 1\,\mathrm{m}^n$; nth moment of a PSD
β signal-to-noise ratio of correlation functions, "intercept"
δ difference angle in cross-correlation techniques; δ_{2C} and δ_{3D} are to be distinguished
η solvent viscosity; $[\eta] = 1\,\mathrm{Pa\,s}$
θ scattering angle
κ inverse Debye screening length, $\kappa^2 = \frac{e^2}{\varepsilon\varepsilon_0 k_B T} \sum_i 1000 \cdot N_L \cdot z_i^2 c_i$; $[\kappa] = 1\mathrm{m}^{-1}$
with
- e elementary charge, $e = 1.602 \cdot 10^{-19}\,\mathrm{Cb}$
- ε dielectric number of the suspending medium, here water, $\varepsilon = 81$
- ε_0 dielectric constant, $\varepsilon_0 = 8.854 \cdot 10^{-12}\,\mathrm{Cb^2\,(N\,m^2)^{-1}}$
- N_L Loschmidt's (Avogadro's) number, $N_L = 6.022 \cdot 10^{23}\,\mathrm{mol}^{-1}$
- z single ion charge

λ wavelength of light in vacuum; $[\lambda] = 1\,\mathrm{m}$
ρ mass density; $[\rho] = 1\,\mathrm{kg\,m}^{-3}$
σ standard deviation of particle radii, polydispersity
τ turbidity; $[\tau] = 1\,\mathrm{m}^{-1}$
τ correlator lag time; $[\tau] = 1\,\mathrm{s}$
ϕ particle volume fraction

8 References

[1] *P. N. Pusey:* Colloidal suspensions, in *J. P. Hansen, D. Levesque, J. Zinn-Justin* (eds.): Liquids, Freezing and Glass Transition. North Holland, Amsterdam 1991, pp. 763–942.

[2] *G. Nägele:* On the dynamics and structure of charge-stabilized suspensions. Physics Rep. *272* (1996) 215–372.

[3] *G. Nägele, M. Watzlawek, R. Klein:* Hard spheres versus Yukawa particles: differences and similarities. Progr. Colloid Polymer Sci. *104* (1997) 31–39.

[4] *K. Schätzel:* Suppression of multiple scattering by photon cross-correlation techniques. J. Modern Optics *38* (1991) 1849–1865.

[5] *H. Lange:* Comparative test of methods to determine particle size and particle size distribution in the submicron range. Part. Part. Syst. Charact. *12* (1995) 148–157.

[6] *N. Garbow, J. Müller, K. Schätzel, T. Palberg:* High-resolution particle sizing by optical tracking of single colloidal particles. Physica A *235* (1997) 291–305.

[7] *P. N. Segrè, W. van Megen, P. N. Pusey, K. Schätzel, W. Peters:* Two-colour dynamic light scattering. J. Modern Optics *42* (1995) 1929–1952.

[8] *E. Overbeck, Ch. Sinn:* Three-dimensional dynamic light scattering. J. Modern Optics *46* (1999) 303–326.

[9] *G. D. J. Phillies:* Suppression of multiple scattering effects in quasielastic light scattering by homodyne cross-correlation techniques. J. Chem. Phys. *74* (1981) 260–262.
G. D. J. Phillies: Experimental demonstration of multiple-scattering suppression in quasielastic-light-scattering spectroscopy by homodyne coincidence techniques. Phys. Rev. A *24* (1981) 1939–1943.

[10] *J. K. G. Dhont, C. G. de Kruif:* Scattered light intensity cross correlation. I. Theory. J. Chem. Phys. *79* (1983) 1658–1663.

[11] *M. Drewel, J. Ahrens, U. Podschus:* Decorrelation of multiple scattering for an arbitrary scattering angle. J. Opt. Soc. Am. A *7* (1990) 206–210.

[12] *L. B. Aberle, S. Wiegand, W. Schröer, W. Staude:* Suppression of multiple scattered light by photon cross-correlation in a 3D experiment. Prog. Colloid Polym. Sci. *104* (1997) 121–125.
L. B. Aberle, P. Hülstede, S. Wiegand, W. Schröer, W. Staude: Effective suppression of multiply scattered light in static and dynamic light scattering. Appl. Opt. *37* (1998) 6511–6524.

[13] *C. Urban, P. Schurtenberger:* Dynamic light scattering in turbid suspensions: an application of different cross-correlation experiments. Progr. Colloid Polym. Sci. *110* (1998) 61–65.
C. Urban, P. Schurtenberger: Characterization of turbid colloidal suspensions using light scattering techniques combined with cross-correlation methods. J. Colloid Interface Sci. *207* (1998) 150–158.

[14] *Ch. Sinn, R. Niehüser, E. Overbeck, T. Palberg:* Dynamic light scattering by preserved skimmed cow milk: a comparison of two-colour and three-dimensional cross-correlation experiments. Progr. Colloid Polym. Sci. *110* (1998) 8–11.

[15] *B. J. Berne, R. Pecora:* Dynamic Light Scattering with Applications to Chemistry, Biology and Physics. Krieger, Malabar 1990.

[16] *E. Overbeck, Ch. Sinn, I. Flammer, J. Rička:* Silicon avalanche photodiodes as detectors for photon correlation experiments. Rev. Sci. Instrum. *69* (1998) 3515–3523.

[17] *I. Flammer, J. Rička:* Dynamic light scattering with single-mode receivers: partial heterodyning regime. Appl. Opt. *36* (1997) 7508–7517.

[18] *P. N. Pusey, R. J. A. Tough:* Particle interactions, in *R. Pecora:* Dynamic Light Scattering, Applications of Photon Correlation Spectroscopy. Plenum Press, New York 1985, pp. 85–179.

[19] *H. C. van de Hulst:* Light Scattering by Small Particles. Dover, New York 1981.

[20] *W. J. Lentz:* Generating Bessel functions in Mie scattering calculations using continued fractions. Appl. Opt. *15* (1976) 668–671.

[21] *Landolt-Börnstein:* Zahlenwerte und Funktionen aus Physik, Chemie, Astronomie, Geophysik und Technik. 6. Auflage, II. Band, 8. Teil: Optische Konstanten. Springer, Berlin 1962 (missing values are linearly interpolated).

[22] *T. Gisler, S. F. Schulz, M. Borkovec, H. Sticher, P. Schurtenberger, B. D'Aguanno, R. Klein:* Understanding colloidal charge renormalization from surface chemistry: experiment and theory. J. Chem. Phys. *101* (1994) 9924–9936.

[23] *U. Apfel, K. D. Hörner, M. Ballauff:* Precise analysis of the turbidity spectra of a concentrated latex. Langmuir *11* (1995) 3401–3407.

[24] *U. Apfel, R. Grunder, M. Ballauff:* A turbidity study of particle interaction in latex suspensions. Colloid Polym. Sci. *272* (1994) 820–829

[25] *J. Lyklema:* Fundamentals of Interface and Colloid Science. Vol. II. Academic Press, London 1993, pp. 3.1–4.135.

[26] *T. Okubo:* Brownian movement of deionized colloidal spheres in gaslike suspensions and the importance of the Debye screening length. J. Phys. Chem. *93* (1989) 4352–4354.

[27] *S. Gorti, L. Plank, B. R. Ware:* Determination of electrolyte friction from measurements of the tracer diffusion coefficients, mutual diffusion coefficients, and electrophoretic mobilities of charged spheres. J. Chem. Phys. *81* (1984) 909–914.

[28] *M. Medina-Noyola, A. Vizcarra-Rendón:* Electrolyte friction and the Langevin equation for charged Brownian particles. Phys. Rev. A *32* (1985) 3596–3605.

[29] *D. N. Petsev, N. D. Denkov:* Diffusion of charged colloidal particles at low volume fraction: theoretical model and light scattering experiments. J. Colloid Interface Sci. *149* (1992) 329–344.

[30] *J. E. Seebergh, J. C. Berg:* Evidence of a hairy layer at the surface of polystyrene latex particles. Colloids Surf. A *100* (1995) 139–153.

[31] *J. W. S. Goossens, A. Zembrod:* Characterisation of the surface of polymer lattices by photon correlation spectroscopy. Colloid Polym. Sci. *257* (1979) 437–438.

[32] *R. W. McDonogh, R. J. Hunter:* The primary electroviscous effect. J. Rheol. *27* (1983) 189–199.

[33] *R. Xu:* Shear plane and hydrodynamic diameter of microspheres in suspension. Langmuir *14* (1998) 2593–2597.

[34] *P. N. Pusey, W. van Megen:* Detection of small polydispersities by photon correlation spectroscopy. J. Chem. Phys. *80* (1984) 3513–3520.

$2K_2 = \overline{\Gamma^2} - \overline{\Gamma}^2 \Leftrightarrow \frac{\sigma^2}{\overline{\Gamma}^2} = \frac{2K_2}{K_1^2}$

für den Filter 2 cf. eq. (1)